Check for updates

View Article Online
View Journal

Green Chemistry

Cutting-edge research for a greener sustainable future

Accepted Manuscript

This article can be cited before page numbers have been issued, to do this please use: Saravanan. Janakiram, L. Ansaloni, S. A. Jin, X. Yu, Z. Dai, R. J. Spontak and L. Deng, *Green Chem.*, 2020, DOI: 10.1039/D0GC00544D.

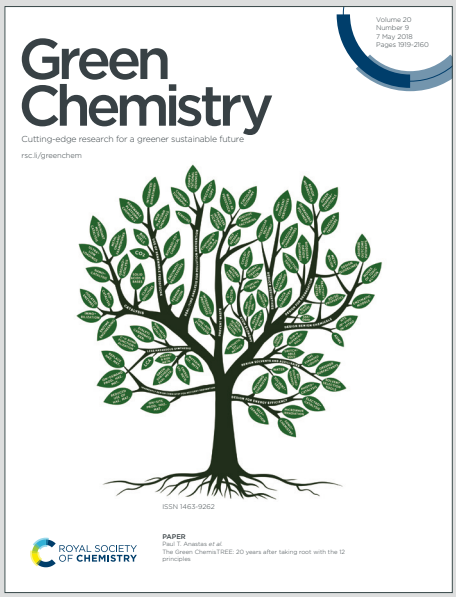

This is an Accepted Manuscript, which has been through the Royal Society of Chemistry peer review process and has been accepted for publication.

Accepted Manuscripts are published online shortly after acceptance, before technical editing, formatting and proof reading. Using this free service, authors can make their results available to the community, in citable form, before we publish the edited article. We will replace this Accepted Manuscript with the edited and formatted Advance Article as soon as it is available.

You can find more information about Accepted Manuscripts in the Information for Authors.

Please note that technical editing may introduce minor changes to the text and/or graphics, which may alter content. The journal's standard Terms & Conditions and the Ethical guidelines still apply. In no event shall the Royal Society of Chemistry be held responsible for any errors or omissions in this Accepted Manuscript or any consequences arising from the use of any information it contains.

ROYAL SOCIETY OF CHEMISTRY

rsc.li/greenchem

View Article Online
DOI: 10.1039/D0GC00544D

Humidity-Responsive Molecular Gate-Opening Mechanism for Gas Separation in Ultraselective Nanocellulose/IL Hybrid Membranes

Saravanan Janakiram,[1] Luca Ansaloni,[2] Soo-Ah Jin,[3] Xinyi Yu,[1] Zhongde Dai,[1] Richard J. Spontak[3,4] and Liyuan Deng[1]*

[1]Department of Chemical Engineering, Norwegian University of Science and Technology Trondheim, 7491, Norway
[2]Department of Sustainable Energy Technology, SINTEF Industry, Oslo, 0373, Norway
[3]Department of Chemical & Biomolecular Engineering, North Carolina State University Raleigh, NC 27695, USA
[4]Department of Materials Science & Engineering, North Carolina State University Raleigh, NC 27695, USA

Published on 06 May 2020. Downloaded by University of Warwick on 5/6/2020 11:12:47 AM.

Green Chemistry Accepted Manuscript

Keywords

Gas-separation membrane; nanofibrillated cellulose; ionic liquid; CO_2 separation; size exclusion

Abstract

Nanofibrillated cellulose (NFC) represents an important class of bio-based nanomaterials that possess favorable properties including hydrophilicity, 1D structure, biodegradability, and surface tunability. Although widely known for its effective gas-barrier attributes due to its inherent crystallinity and hydrogen-bonding capability, the ability of NFC to form dense films has been of considerable interest in selective gas-separation applications as a viable replacement for synthetic polymers. With precise control of targeted properties at the nanoscale, NFC can likewise be used to enable selective removal of greenhouse gases such as CO_2. Herein we report a class of "green" hybrid membranes composed of NFC and an ionic liquid (IL), 1-ethyl-3-methylimidazolium acetate ([Emim][OAc]) that together exhibit exceptional separation properties arising from controllable nanoscopic design. With this new class of green membranes, CO_2/N_2 selectivities as high as ~370 and CO_2 permeabilities as high as ~330 Barrer have been obtained at optimal IL loadings and/or humidity levels. The current work demonstrates that size exclusion of a molecular penetrant in a water-swollen NFC membrane matrix relies on the network architecture of partially swollen nanocellulose fibrils to selectively permeate CO_2 through enhanced diffusive pathways. Additionally, the gas-transport and rheological properties of these NFC-fabricated membranes can be precisely tuned through the independent use of humidity as an external control parameter.

* To whom correspondence should be addressed (e-mail: liyuan.deng@ntnu.no).

View Article Online
DOI: 10.1039/D0GC00544D

Table of Contents Graphic

A class of "green" hybrid membranes composed of nanocellulose and an ionic liquid exhibits exceptional separation properties arising from a humidity-responsive size-exclusive "gate" that allows selective CO_2 permeation.

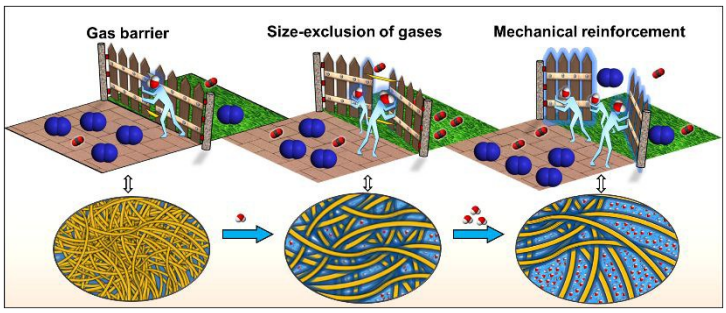

Published on 06 May 2020. Downloaded by University of Warwick on 5/6/2020 11:12:47 AM.

Green Chemistry Accepted Manuscript

View Article Online
DOI: 10.1039/D0GC00544D

Published on 06 May 2020. Downloaded by University of Warwick on 5/6/2020 11:12:47 AM.

Green Chemistry Accepted Manuscript

Introduction

Due to its relatively low cost, biodegradability and nanostructural tunability, nanocellulose, including nanofibrillated cellulose (NFC), cellulose nanocrystals (CNC) and bacterial nanocellulose (BNC), constitutes a valuable building block for many advanced material designs in a wide variety of contemporary applications.[1] As a consequence of its abundant availability and natural renewability coupled with its inherently high crystallinity and hydrogen-bonding propensity that promotes the formation of films with excellent gas-barrier properties, nanocellulose is of greatly escalating interest as an eco-friendly and biodegradable alternative to synthetic, oil-derived plastics in packaging industries.[2,3] However, little is known about using such bio-based nanomaterials for gas-separation applications, especially those targeting CO_2 capture for the mitigation of climate change.[4] Ansaloni *et al*.[5] and Venturi *et al*.[6] have investigated NFC in the form of pristine films, as well as nanocomposite membranes containing poly(vinyl amine) (PVAm), for CO_2 separation. In the latter case, the high hydroxyl density on the surface of NFC ensures compatibility with hydrophilic polymers to achieve satisfactory mechanical reinforcement,[5,7] whereas PVAm permits facilitated transport of CO_2 in the presence of fixed-site carriers. The NFC likewise increases water retention, thereby promoting superior CO_2 transport in these nanocomposite membranes. Similar results have been obtained in our previous works wherein nanocellulose was found to benefit CO_2 transport in nanocomposite membranes containing NFC nanofillers in various polymeric matrices.[4,8,9] However, the CO_2 permeability of neat NFC films in the absence of polymer matrix is very low due to the presence of discrete crystalline obstacles[10] distributed throughout the membranes,[5] even though these neat NFC membranes may exhibit high CO_2 selectivities relative to both N_2 and CH_4 under humid conditions. Moreover, interfibrillar hydrogen bonding renders pristine NFC membranes brittle and thus mechanically unsuitable for commercial gas-separation applications. Nonetheless, its semicrystalline structure is composed of amorphous

View Article Online
DOI: 10.1039/D0GC00544D

lignin and hemicellulose domains that can favor specific gas permeation.[1,5,11] Introduction of NFC-compatible CO_2-philic additives is therefore anticipated to result in bio-based hybrid membranes that possess high CO_2 solubility.

In the present study, the gas-permeation performance of NFC films is improved through the addition of an ionic liquid (IL), which serves to enhance CO_2 solubility for more effective separation. Prior studies have examined[12–14] the thermodynamic compatibility of ILs with different cellulosic materials, and resultant cellulose/IL blends typically possess interesting CO_2-separation properties due largely to the presence of the IL.[15] Combining these attributes, we posit that the NFC semicrystalline network can be exploited as a physical barrier for nonspecific gases while IL-swollen regions permeate CO_2. In this scenario, humidity can provide another independent degree of freedom, since water synergistically interacts with hydrophilic ILs[16,17] and NFC,[18] to allow precise control over CO_2 transport through IL-containing hybrid membranes under isothermal conditions. In the spirit of molecular size sieving, numerous inorganic membranes or polymer nanocomposites containing nanoporous metal-organic frameworks (MOFs) or zeolite inclusions have been developed.[19–22] In these cases, highly selective gas transport is achieved by judicious design of the nanopores in the fillers prior to fabrication as membranes. In marked contrast, we fabricate hybrid NFC/IL membranes and subsequently employ the nanofibrillar network of NFC to induce a comparable size-sieving effect that is tunable under humid conditions. By doing so, we find that the CO_2 selectivity remains high, whereas the CO_2 permeability escalates by a factor of over 12x relative to neat NFC films, thereby exceeding the Robeson upperbound[23] for CO_2 in the presence of N_2. These hybrid membranes are predominantly bio-based, highly sustainable and eco-friendly, completely avoiding synthetic polymers and toxic solvents. The current work also demonstrates a unique humidity-controlled "gate-opening" transport mechanism that promotes molecular selectivity in water-swollen NFC/IL membranes.

Published on 06 May 2020. Downloaded by University of Warwick on 5/6/2020 11:12:47 AM.

Green Chemistry Accepted Manuscript

View Article Online
DOI: 10.1039/D0GC00544D

Published on 06 May 2020. Downloaded by University of Warwick on 5/6/2020 11:12:47 AM.

Green Chemistry Accepted Manuscript

Experimental

Materials

The NFC, originated from eucalyptus pulp, was provided by INOFIB S.A.S. (France) as a suspension in water at a solids content of 3.3 wt%. 1-Ethyl-3-methylimidazolium acetate ([Emim][OAc], 97%) was purchased from Sigma-Aldrich (Norway) and used as-received. The gases investigated in permeation tests included a CO_2/N_2 mixture (10/90 v/v CO_2/N_2) and several pure gases — He (99.99%), N_2 (99.999%) and CH_4 (99.95%) — all of which were purchased from AGA (Norway). Gas-separation support membranes composed of polydimethylsiloxane (PDMS) on polyacrylonitrile (PAN) were provided by Fujifilm Europe B.V. (The Netherlands).

Fabrication

Both NFC membranes and hybrid NFC/IL membranes were fabricated in this work. The IL loading levels considered were 20, 35 and 50 wt% [Emim][OAc] relative to the solids content of the membranes. For each NFC/IL membrane, a predetermined quantity of IL was added to an aqueous NFC suspension to achieve a given blend composition. The suspension was then continuously stirred for 1-2 days to ensure homogeneous NFC dispersion. Self-standing NFC-based membranes were prepared by casting the aqueous suspension in a Teflon Petri dish, followed by quiescent solvent evaporation in a convection oven maintained at 40°C. The thickness of the resulting films varied from 35 to 60 μm. To generate thin membranes suitable for permeation tests, aqueous NFC and NFC/IL suspensions were cast and subjected to vacuum filtration on PDMS/PAN support membranes, yielding a dense surface layer about 2 μm thick. Self-standing membranes were examined by a battery of characterization methods and single-gas permeation tests, whereas thin membranes were investigated by mixed-gas permeation tests.

View Article Online
DOI: 10.1039/D0GC00544D

Published on 06 May 2020. Downloaded by University of Warwick on 5/6/2020 11:12:47 AM.

Green Chemistry Accepted Manuscript

Characterization

Morphological analysis of membrane surfaces and cross-sections was performed by scanning electron microscopy (SEM) in a Hitachi TM3030 microscope. Membrane samples were cryofractured in liquid nitrogen for cross-sectional analysis. To improve conductivity, all samples were sputter-coated with a few nanometers of Au in Ar prior to analysis. Secondary and back-scattered electrons were acquired at accelerating voltages of either 5 or 15 kV. Swollen NFC in the presence of IL was analyzed by S(T)EM, SEM and energy-dispersive X-ray spectroscopy (EDS) in a Hitachi S-5500 scanning transmission electron microscope equipped with an in-lens cold field-emission source and a Bruker X-ray detector. Specimens were prepared by dropping dilute (0.1 wt%) NFC suspensions onto 300-mesh Cu support grids, followed by washing twice with deionized (DI) water. For surface composition analysis, X-ray photoelectron spectroscopy (XPS) was conducted on a Thermo Fisher Scientific XPS-Theta system outfitted with a monochromatic Al Kα source. The chemical signature of all specimens was analyzed by Fourier-transform infrared (FTIR) spectroscopy performed in attenuated total reflectance (ATR) mode on a Thermo-Nicolet Nexus spectrometer equipped with a smart endurance reflection cell and a diamond crystal. Spectra were averaged over 16 scans at a resolution of 4 cm^{-1}. The thermal properties of self-standing films were interrogated by thermogravimetric analysis (TGA) conducted on a TG 209 F1 Libra instrument. Each specimen was heated from ambient temperature to 800°C at a heating rate of 10°C/min under a N_2 purge at a flow rate of 60 ml/min. Accompanying water contact angles of membranes were discerned with a Biolin Scientific Attension Theta contact-angle goniometer. Measurements reported as the average between opposing initial contact angles used a 2 μL drop of water.

The water uptake capacity of the NFC/IL hybrid membranes was measured at 35°C by the pressure-decay apparatus described elsewhere.[24] A measured mass of dry sample was placed in an isolated volume (35.1 ± 0.2 cm^3) maintained under vacuum to completely evacuate

View Article Online
DOI: 10.1039/D0GC00544D

dissolved penetrants, and another closed volume chamber (49.7 ± 0.2 cm^3) was saturated with water at a specific vapor pressure, monitored by a pressure sensor. After stabilizing the water vapor pressure in the second volume, both chambers were brought into contact. The gradual decline in pressure due to water uptake by the sample was recorded over time and correlated with respect to water activity.[4,5,25,26] In addition, the mass uptake (M_t) evaluated at a given time (t) was used to estimate the diffusivity of water (D) according to Fick's law:[27]

$$\frac{M_t}{M_\infty} = 1 - \frac{8}{\pi^2}\sum_{n(2n+1)^2}\frac{1}{}\exp\left[-(2n+1)^2\left(\frac{\pi}{L}\right)^2 Dt\right] \quad (1)$$

where M_∞ represents the mass measured at infinite time (the solubility), and L is the specimen thickness. Values of D were obtained by the best fit of **Eq. 1** to experimental data at relatively short times under the assumption that, compared to the initial sample state, no significant chain relaxation occurs at low water concentration in the membrane matrix. Therefore, pseudo-Fickian diffusion was presumed here to avoid complications associated with the kinetics of chain relaxation, as described elsewhere.[5] Films were analyzed for dry CO_2 and N_2 sorption at elevated pressures in a TA Instruments Rubotherm IsoSORP gravimetric balance. To ensure a dry mass prior to loading, each specimen was held under an external vacuum for 24 h, after which the magnetic suspension balance was exposed to the internal vacuum until the mass reading was constant (indicating complete evacuation of dissolved penetrants). The pressure was increased incrementally and isothermal sorption measurements were performed at 35°C. Dry He tests yielded the sample volume required to counteract buoyancy changes inside the chamber. Complementary property analyses are provided in the **Supporting Information**.

Both single-gas and mixed-gas permeation tests were performed to effectively characterize the gas separation performance of fabricated hybrid membranes. Single-gas permeabilities of CO_2, N_2 and CH_4 through the NFC/IL membranes were measured using the humid single-gas permeation setup, as schematically depicted in **Figure 1**. Each hybrid membrane was

Published on 06 May 2020. Downloaded by University of Warwick on 5/6/2020 11:12:47 AM.

Green Chemistry Accepted Manuscript

View Article Online
DOI: 10.1039/D0GC00544D

sandwiched between two pieces of impermeable Al tape and sealed with epoxy glue. The specimen was then placed in the membrane module, and the whole system was evacuated to ensure removal of any volatile species. The membrane was subsequently stabilized at a specified water activity using water vapor obtained from a liquid water tank at a particular vapor pressure to ensure that the membrane was at a target relative humidity (RH). Concurrent streams of fully saturated gas (obtained by bubbling through the liquid water tank) and dry gas were mixed to generate a gas stream of particular relative humidity by controlling individual mass flows. The temperature, RH and pressure in the downstream were continuously monitored by an integrated sensor (HygroFlex HF5, ROTRONIC) and an absolute capacitance manometer (MKS, Baratron), respectively. Upon opening the V5 valve in **Figure 1**, the upstream side of the membrane was exposed to a constant flow of gas humidified at constant RH (corresponding to the value at which the membrane is equilibrated) and 1 bar. Under these conditions, the driving force for water-vapor permeation is negligible. The increase in downstream pressure can be exclusively attributed to incoming incondensable gas that permeates through the membrane.[28] At steady state (time-independent pressure variation), the permeability (P) of a single-gas was calculated from the constant-volume variable-pressure method according to

$$P = \frac{V_d L}{RTA(p_u - p_d)}\left(\frac{dp_d}{dt}\right) \quad (2)$$

Here, $\left(\frac{dp_d}{dt}\right)$ is the leak-corrected pressure variation over time measured by the pressure transducer, V_d is the downstream volume, p_u and p_d represent upstream and downstream pressures, respectively, R is the universal gas constant, T denotes absolute temperature, and A corresponds to the exposed membrane area. Permeability values calculated by **Eq. 2** are reported here in Barrer, where 1 Barrer = 10^{-10} cm^3(STP) cm^{-1} s^{-1} cm Hg^{-1} = 3.35 x 10^{-16} mol m^{-1} s^{-1} Pa^{-1}. The ideal selectivity between gases i and j (α_{ij}), a metric of the quality of gas separation, is defined as P_i/P_j.

Published on 06 May 2020. Downloaded by University of Warwick on 5/6/2020 11:12:47 AM.

Green Chemistry Accepted Manuscript

View Article Online
DOI: 10.1039/D0GC00544D

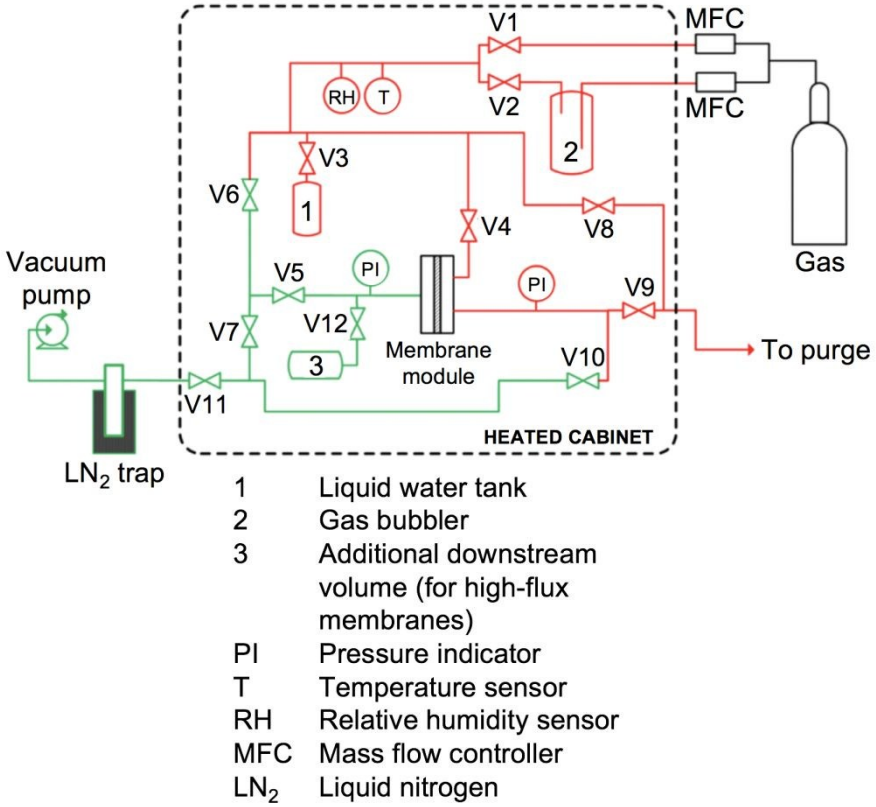

Figure 1. Schematic illustration of the single-gas permeation setup used for measuring pure-gas permeabilities in the presence of controllable relative humidity (RH).

An in-house mixed-gas permeation setup with humidity control was used to perform the mixed-gas permeation tests. Detailed technical information about this set-up and the test procedure was reported earlier.[4] Mixed-gas measurements yielded the actual permeation of a gas mixture for realistic gas-separation performance assessment. In this case, a thin membrane with a dense selective layer was coated on a support membrane for analysis. A circular section cut from each membrane was placed inside a sample holder in which the permeate area varied from 2.0 to 2.5 cm^2 due to masking prior to measurement. The membrane was stabilized with regard to both humidified sweep and feed gases. In these tests, the feed gas was a CO_2/N_2 gas mixture (mimicking flue gas), whereas the sweep gas was pure CH_4. Constant RH was achieved by controlling the dry and humidified gas flows. The feed pressure was regulated to 1.7 bar in the upstream by a back-pressure regulator, and the sweep side was maintained at 1.05 bar. A calibrated Agilent 490 Micro gas chromatograph was used to analyze the composition of the

Published on 06 May 2020. Downloaded by University of Warwick on 5/6/2020 11:12:47 AM.

Green Chemistry Accepted Manuscript

View Article Online
DOI: 10.1039/D0GC00544D

retentate, permeate and feed streams at steady-state conditions, and the permeability of the ith gas was calculated from

$$P = \frac{\dot{V}_p(1 - y_{H_2O})y_i L}{((p_{i,f} - p_{i,r}) - p_{i,p})A} \quad (3)$$

Here, $\dot{V}_p$ represents the total permeate flow rate measured at steady state, y_{H_2O} and y_i are the mole fractions of water and gas *i*, respectively, in the permeate, and $p_{i,f}$, $p_{i,r}$ and $p_{i,p}$ correspond to the partial pressures of gas *i* in the feed, retentate and permeate, respectively. The associated separation factor ($\alpha_{i/j}$) is given by

$$\alpha_{i/j} = \frac{y_i/x_i}{y_j/x_j} \quad (4)$$

where y_k and x_k ($k = i$ or j) are the mole fractions of gas k in the permeate and retentate, respectively.

Results and Discussion

Morphological characteristics

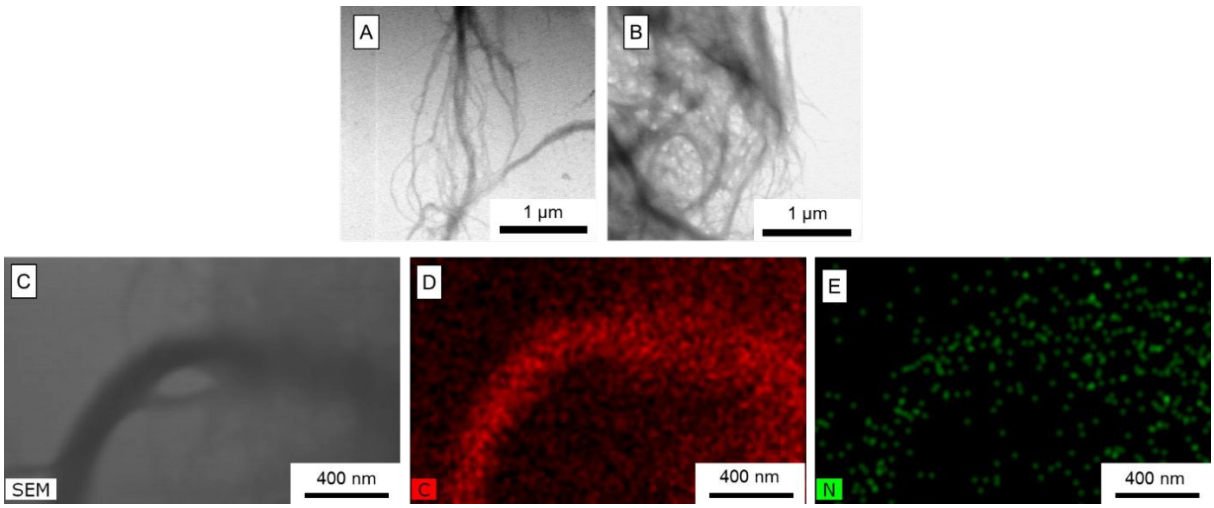

Figure 2. S(T)EM images of (A) neat NFC fibrils and (B) NFC fibrils containing IL. In (C), a higher-resolution SEM image of NFC with spatially-correlated IL, as evidenced by elemental mapping of carbon (D) indicative of NFC and nitrogen (E) indicative of the IL.

To discern the nanofibrillar morphology and chemical composition of NFC in the presence

Published on 06 May 2020. Downloaded by University of Warwick on 5/6/2020 11:12:47 AM.

Green Chemistry Accepted Manuscript

View Article Online
DOI: 10.1039/D0GC00544D

of the [Emim][OAc] IL, STEM-EDS analysis has been performed, and representative results are presented in **Figure 2**. These findings have been obtained by first dropping a highly diluted aqueous suspension of NFC containing 35 wt% [Emim][OAc] on a Cu support grid positioned on soft tissue to remove excess liquid and then adding additional DI water to remove excess IL and leave behind IL that is chemically attached to the NFC. Randomly entangled nanofibrillar clusters characteristic of NFC[4] are observed, thereby confirming no physical changes to the NFC morphology triggered by the addition of IL. Corresponding EDS maps of the NFC bundles reveal that the spatial distribution of IL is correlated with that of the NFC, as verified by the N map in **Figure 2** (since NFC does not contain N). Moreover, according to XPS results (*cf.* **Figure S1** in the **Supporting Information**), addition of IL increases the surface C:N:O ratio from 0.58:0.00:0.42 to 0.57:0.03:0.42 in the case of 20% [Emim][OAc] and 0.58:0.05:0.37 in the case of 35% [Emim][OAc]. This spatial correlation of [Emim][OAc] with NFC nanofibrils is consistent with the expected compatibility of IL with the hydroxyl-rich surface of NFC. It immediately follows that the interaction between IL acetate ions with NFC hydroxyl groups, along with re-orientation of imidazolium rings in close proximity to the NFC surface,[29] most likely disrupts hydrogen-bonding between adjacent nanofibrils and thus loosens the NFC network. It is reasonable to assume that surface coverage of individual nanofibrils by IL reduces the capacity of NFC nanofibrils to form very tightly connected networks through interfibrillar hydrogen bonding, thus softening the films.[30] From a gas-transport perspective, surface anchoring of [Emim][OAc] is additionally beneficial for CO_2 transport by promoting surface diffusion through the imidazolium moieties, since the crystals present in NFC nanofibrils act as physical barriers to gas transport.

Published on 06 May 2020. Downloaded by University of Warwick on 5/6/2020 11:12:47 AM.

Green Chemistry Accepted Manuscript

View Article Online
DOI: 10.1039/D0GC00544D

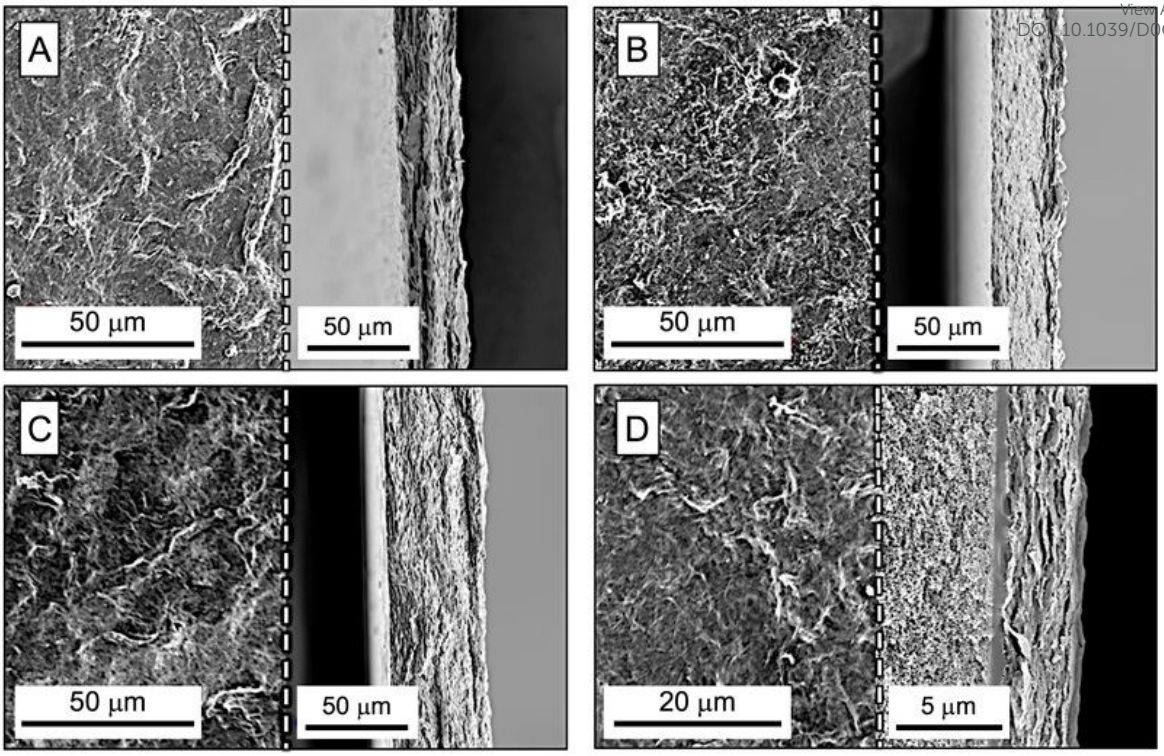

Figure 3. SEM images of film surfaces (left of white dashed line) and cross-sections (right of white dashed line) acquired from specimens with different levels of added [Emim][OAc] IL (in wt%): (A) 0, (B) 20, (C) 35, and (D) 50. The 50% IL-containing sample is obtained as a thin-film membrane on a PDMS/PAN composite support.

The inherent ability of NFC nanofibrils to physically connect and form tight networks stabilized by hydrogen-bonding is responsible for promoting the formation of defect-free films suitable for gas-barrier applications such as packaging. Solvent-cast films are characterized by layered structures composed of randomly oriented nanofibrils, as generally observed for specimens varying in IL loading level in **Figure 3**. This topology is characteristic of NFC films due to random in-plane orientation.[31] As reported by Svagen *et al.*,[32] hydrogen-bonding between nanofibrils in a single layer (intralayer interaction) is stronger than that between nanofibrils residing in different layers (interlayer interaction). For this reason, the cryofractured planar surface of neat NFC in **Figure 3A** appears rough due to the widespread protrusion of discretely bound NFC layers that remain mechanically intact.[33] When [Emim][OAc] is added to the dispersion, the IL coats the NFC nanofibrils and, by doing so, successfully precludes both intralayer and interlayer hydrogen-bonding during solvent drying. While disruption of

Published on 06 May 2020. Downloaded by University of Warwick on 5/6/2020 11:12:47 AM.

Green Chemistry Accepted Manuscript

View Article Online
DOI: 10.1039/D0GC00544D

NFC hydrogen-bonding induced by the addition of IL has a slightly discernible effect on fracture topology (*cf.* **Figures 3B-D**), it strongly affects hybrid NFC/IL films with 20 and 35 wt% [Emim][OAc]. According to DMA, the dynamic storage tensile modulus of NFC decreases (*cf.* **Figure S2** in the **Supporting Information**) as the NFC crystallinity, as measured by XRD, decreases (*cf.* **Figure S3** in the **Supporting Information**) in the presence of IL.

Chemical and thermal properties

Chemical interactions between NFC nanofibrillar surfaces and the IL have been examined by FTIR spectroscopy performed in ATR mode. Representative spectra of NFC, the IL and hybrid NFC/IL membranes are displayed for comparison in **Figure 4A**. A key chemical signature of native cellulose is the existence of a broad peak between 3250 and 3690 cm^{-1} attributed to -OH stretching associated with both intramolecular and intermolecular hydrogen-bonding. Additional sharp peaks are positioned at 1060 and 2880 cm^{-1} due to C-O-C and symmetric C-H stretching, respectively, of cellulosic chains[34]. Pristine [Emim][OAc] IL is differentiated by the presence of symmetric O-C-O stretching at 1380 cm^{-1} and asymmetric O-C-O stretching at 1566 cm^{-1}, in addition to symmetric C=N stretching in the imidazolium ring at 1001 cm^{-1}. Interactions between IL and the NFC nanofibrils are identified by upward shifts in the spectral peak initially at 1380 cm^{-1} due to the formation of hydrogen bonds between acetate ions on the IL and cellulose hydroxyl groups on the NFC. Moreover, a shift in the peak position related to CO stretching at 1174 cm^{-1} provides evidence of additional intermolecular hydrogen bonding.[30] Except for these indicators of hydrogen-bonding interactions between the NFC and IL, no new bonds could be detected from these spectra, thus confirming no permanent chemical modification to the nanofibrillar surfaces.

Published on 06 May 2020. Downloaded by University of Warwick on 5/6/2020 11:12:47 AM.

Green Chemistry Accepted Manuscript

View Article Online
DOI: 10.1039/D0GC00544D

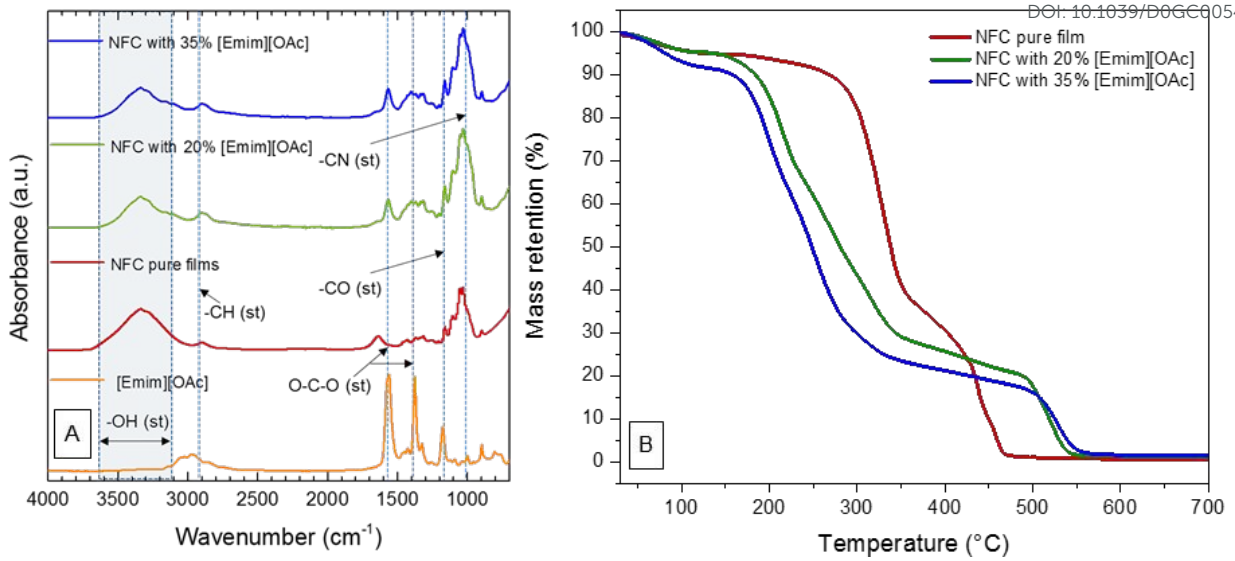

Figure 4. (A) FTIR spectra acquired from NFC, [Emim][OAc] and hybrid NFC/IL films containing different loading levels of [Emim][OAc] (labeled and color-coded). (B) Mass-loss measurements acquired by TGA from pristine NFC and two hybrid NFC/IL films (see legend for specimen details).

Imidazolium-based ionic liquids often possess relatively low melting points, in which case the addition of [Emim][OAc] is expected to decrease the thermal stability of NFC films. To ascertain the extent of this anticipated outcome, we have performed TGA on NFC and hybrid NFC/IL films, and the results are provided in **Figure 4B**. An initial mass loss at about 100ºC in all three specimens examined is attributed to loss of water. Interestingly, this reduction is nearly identical for neat NFC and NFC containing 20 wt% IL. At the higher IL loading level examined here (35 wt%), this feature is more pronounced, implying that the hydrophilic IL likewise contains water. These differences are in favorable agreement with the water-uptake measurements discussed below. The degradation onset temperature at which a precipitous drop in mass occurs is observed at just over 300°C for pure cellulose nanofibrils, which reflects their high degree of internal hydrogen-bonding, as well as their aromatic nature. Incorporation of IL disrupts and reorients the surface hydroxyl groups of the nanofibrils to prevent interfibrillar hydrogen-bonding, thereby promoting a considerable reduction in the thermal stability of NFC/IL films to less than 200°C: ~198ºC for NFC with 20 wt% IL and ~180ºC for NFC with 35 wt% IL. It is important to recognize that the initial degradation onset temperature of

Published on 06 May 2020. Downloaded by University of Warwick on 5/6/2020 11:12:47 AM.

Green Chemistry Accepted Manuscript

View Article Online
DOI: 10.1039/D0GC00544D

[Emim][OAc] is 215ºC.[35] The mechanism of expedited degradation in the NFC/IL films is attributed to S_N2 nucleophilic attack of acetate ions on the alkyl chain of [Emim][OAc], which, in turn, leads to scission of both the IL and the cellulose backbone. Since an increase in IL loading in NFC decreases both the specific heat capacity and viscosity of the blend, anion mobility is accelerated throughout the matrix, thereby facilitating alkyl chain and cellulosic degradation,[14] with increasing temperature. Although the initial degradation temperature of NFC/IL films is depressed upon incorporation of IL, these hybrid films (unlike NFC) become relatively stable at about 350°C and undergo a second degradation event at ~500°C. Above *ca*. 550°C, all the films (including pure NFC and NFC/IL blends) yield virtually no residual ash.

Water sorption

Water plays a major role in the nanoscale swelling of NFC,[36] as well as the transport of CO_2 through NFC-based membranes.[4,5,9] The hydrophilicity of the hybrid membranes produced here is anticipated to increase as the concentration of incorporated IL is increased. This expectation is corroborated from initial water contact-angle measurements: 37° for neat NFC films, but 26° and 19° upon addition of 20% and 35% [Emim][OAc], respectively. Moreover, a pressure-decay apparatus described elsewhere[4] is used to monitor the water-uptake capacity of each test specimen and yields the water per polymer mass (in g/g_{pol}) as a function of water activity (obtained from p/p^{sat}, where p and p^{sat} represent the measured and saturated pressure of water vapor at 35°C). Representative results obtained from pure NFC and two NFC/IL films are presented in **Figure 5A**. Sigmoidal sorption curves are observed for all the materials examined, which is consistent with the swelling behavior of hydrophilic cellulose.[18] Addition of IL systematically enhances the water uptake of NFC films according to the IL loading level: from 0.06 g/g_{pol} for pure NFC to 0.11 g/g_{pol} at 20 wt% [Emim][OAc] and 0.21 g/g_{pol} at 35 wt% [Emim][OAc], all measured at a water activity of 0.6. As the data shown in **Figure 5A** indicate, this water-uptake change increases with increasing water activity. At higher water activities,

Published on 06 May 2020. Downloaded by University of Warwick on 5/6/2020 11:12:47 AM.

Green Chemistry Accepted Manuscript

View Article Online
DOI: 10.1039/D0GC00544D

water clustering is expected in NFC-based membranes,[4,18] thereby leading to an exponential increase in water uptake at high humidity conditions. In addition to water uptake, sorption measurements have also been correlated to the kinetics of water uptake at each pressure increment and confirm Fickian diffusion according to the mathematical procedure proposed by Minelli *et al*.[18] and Ansaloni *et al*.[5]

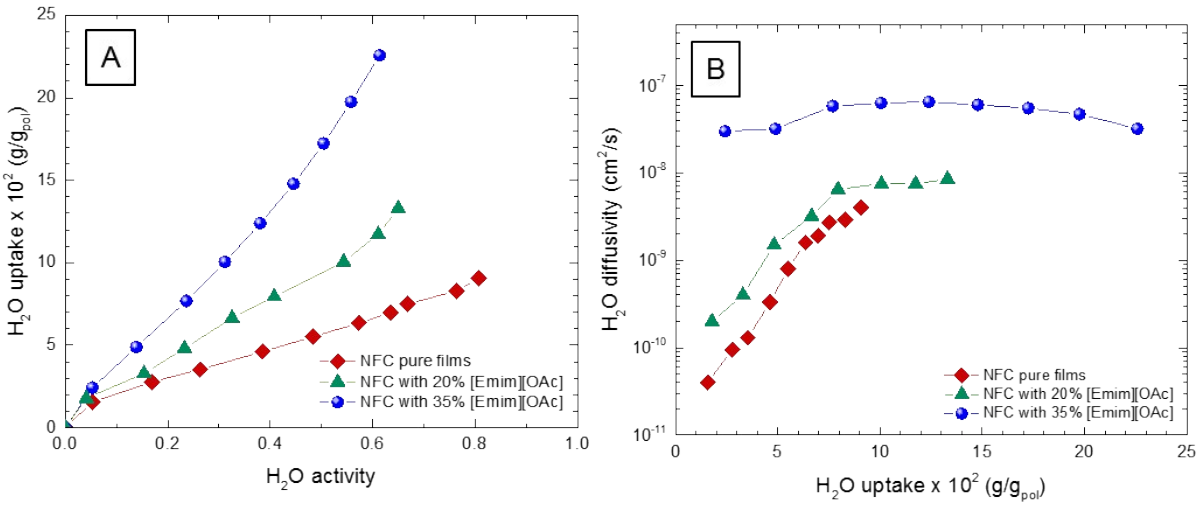

Figure 5. (A) Water uptake and (B) Fickian water diffusivities measured at 35°C for pristine NFC and hybrid NFC/IL films (see legends for specimen details). The solid lines serve to connect the data.

In **Figure 5B**, water diffusivity in neat NFC films increases with increasing water uptake in the pristine NFC matrix. For example, as the water uptake is increased from 0.016 to 0.090 g/g_{pol}, the corresponding water diffusivity increases by two orders of magnitude (from ~4 x 10^{-11} to ~4 x 10^{-9} cm^2/s). This correlation is attributed to NFC swelling due to the inherent hydrophilicity of nanocellulose. Hybrid NFC/IL films, on the other hand, display pronounced differences even at low water activities where swelling is expected to be less effective. At low RH levels, water orients and localizes along the aromatic protons in the imidazolium ring of [Emim][OAc].[37] The high water diffusivity at low RH in the NFC/IL films with 35 wt% [Emim][OAc] is attributed to anisotropic cation diffusion and water surface diffusion through IL pathways. Even at such low loading levels, the IL conduit is sufficiently contiguous for

Published on 06 May 2020. Downloaded by University of Warwick on 5/6/2020 11:12:47 AM.

Green Chemistry Accepted Manuscript

View Article Online
DOI: 10.1039/D0GC00544D

water molecules to diffuse along NFC interfaces without requiring much bulk swelling. This can be attributed to the hydrophilicity of both IL and NFC and the smaller kinetic diameter of water molecules. Hence, in this case, the diffusivity of water is significantly higher (~3 x 10^{-8} cm^2/s) than it is in NFC/IL films containing 20 wt% [Emim][OAc] (~4 x 10^{-10} cm^2/s) at a constant water uptake level of 0.024 g/g_{pol}. At higher water activity levels, faster diffusion results in a maximum water diffusivity of ~7 x 10^{-8} cm^2/s at a water activity of 0.4 in NFC/IL films containing 35 wt% [Emim][OAc] (*cf.* **Figure 5**). A similar maximum occurs at ~9 x 10^{-9} cm^2/s in films with 20 wt% [Emim][OAc] at a water activity of 0.65. If the activity is increased further in both instances, however, the water diffusivity is observed to drop since water can diffuse through bulk channels as dimers and trimers, along with hydrated ions associated with the IL regions.

Gas permeation

Humid single-gas permeation tests have been performed on membranes at three different RH levels, namely, 30, 60 and 90% at 35ºC, and the results are provided in **Figure 6**. According to this figure, the CO_2 permeability of NFC/IL membranes increases substantially with increasing RH due presumably to increased water uptake in the NFC matrix (*cf.* **Figure 5A**). Although NFC usually acts as a barrier material to gas permeation because of its high crystallinity arising from hydrogen-bonding, the dual presence of IL and water promotes both enhanced CO_2 sorption and diffusion, thereby increasing CO_2 permeation. While the introduction of IL promotes an increase in CO_2 permeation at all RH levels,[17] vastly different behavior is encountered with regard to the permeation of N_2, thereby yielding an unexpectedly high ideal selectivity of CO_2 relative to N_2 at intermediate humidity levels. At *ca*. 60% RH, the CO_2/N_2 ideal selectivity increases sharply to up to ~410 for NFC/IL membranes containing 35 wt% [Emim][OAc] and then decreases sharply at higher humidification levels. A similar, albeit less pronounced (~150), ideal selectivity maximum is also evident in the case of NFC/IL

Published on 06 May 2020. Downloaded by University of Warwick on 5/6/2020 11:12:47 AM.

Green Chemistry Accepted Manuscript

membranes with 20 wt% [Emim][OAc].

View Article Online
DOI: 10.1039/D0GC00544D

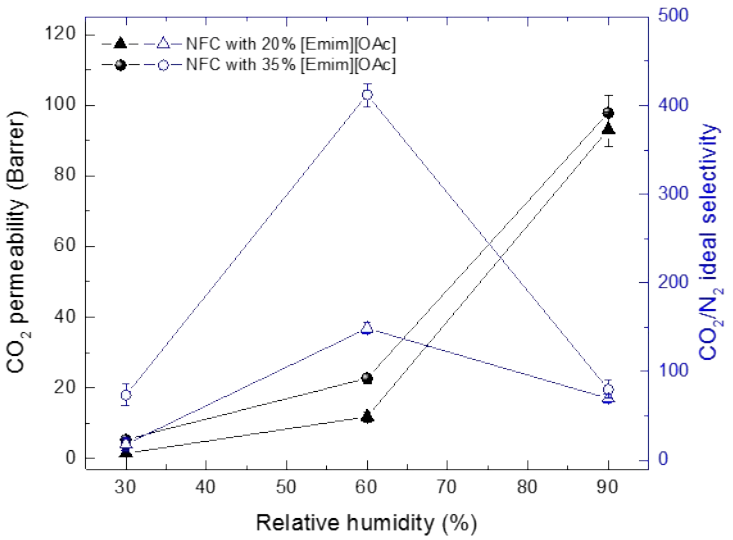

Figure 6. Single-gas CO_2 permeability (black, left axis) and CO_2/N_2 ideal selectivity (blue, right axis) for two hybrid NFC/IL membranes (see legend for specimen details) presented as functions of RH measured at 35°C and 1 bar. The solid lines serve to connect the data, and the error bars correspond to the standard error in the data.

The interaction of CO_2 with a humidified membrane is reportedly[5,38] dependent on water activity in the corresponding matrix. In addition, the chemical composition of the membrane matrix strongly affects CO_2 transport across the membrane as both gas molecules and dissolved species. First, the acetate ions of the IL strongly interact through hydrogen-bonding with the nanofibrillar surfaces, thus reducing interfibrillar interactions and enhancing the available surface area of the nanofibrils for both water and CO_2 sorption. Previous studies[4,9] have concluded that CO_2 interacts with nanocellulose surfaces due to charge affinity. In fact, CO_2 can weakly complex with acetate anions via a reversible bond that could improve the surface diffusion of CO_2 along the nanofibrillar surfaces.[39] Moreover, chemisorption of CO_2 on dry imidazolium-based ILs has been found[40] to induce CO_2 complexation contributing to enhanced sorption, and the introduction of water triggers rapid release of chemically sorbed CO_2 and expedites the production of bicarbonate species from the same complex.

Another nontrivial effect is related to the reduction of IL viscosity in the presence of water, which serves to enhance the diffusion of small molecules such as CO_2 through water-swollen

Published on 06 May 2020. Downloaded by University of Warwick on 5/6/2020 11:12:47 AM.

Green Chemistry Accepted Manuscript

View Article Online
DOI: 10.1039/D0GC00544D

IL domains.[41,42] At high humidity levels, the contiguous IL/water channels provide a fast diffusive pathway for hydrated complexes, in addition to the transport of free CO_2. It should be recognized that these channels can also physically transport other species such as CH_4 and He. Under the present experimental conditions, the permeability of CO_2 increases remarkably with increasing water content in the NFC matrix. The permeation behavior of CO_2 apparent in **Figure 6** from single-gas measurements is likewise observed in mixed-gas tests (*cf.* **Figure 7**) wherein the permeability of CO_2 increases to a maximum of ~320 Barrer in hybrid NFC/IL membranes with 50 wt% [Emim][OAc] at 90% RH and 35ºC. Interestingly, at this RH level, the CO_2 permeabilities of NFC/IL membranes containing either 35 or 50 wt% [Emim][OAc] are similar, suggesting that the continuous IL/water-rich channels responsible for fast CO_2 diffusion exist at the lower IL loading level, in which case the CO_2 permeabilities are more than 12x greater than that achieved in neat NFC membranes without the addition of IL.

Another observation that warrants discussion is that the CO_2/N_2 selectivity measured in both single- and mixed-gas tests are qualitatively comparable with a pronounced peak (at ~60% RH) relative to values recorded at lower and higher humidity levels. To identify the origin of such high selectivity, we have performed sorption tests aimed at decoupling the solubility and diffusivity coefficients for gaseous CO_2 and N_2. At low CO_2 pressures in particular, the effect of IL loading on CO_2 solubility is measurable but not significant (*cf.* **Figure S4A** in the **Supporting Information**), which indicates that CO_2/N_2 solubility selectivity (*cf.* **Figure S4B** in the **Supporting Information**) in NFC/IL membranes is not the dominant contributor to the high CO_2/N_2 selectivity measured in single- and mixed-gas permeation tests. Although the interactions of CO_2 can be different in the presence of water, however, the semicrystalline nanocellulose network still serves as a barrier to non-interacting gases and its effectiveness varies as a function of RH. This well-established attribute of NFC nanofibrils, along with the aforementioned low sorption selectivity of CO_2 in the NFC/IL membrane, implies that the

Published on 06 May 2020. Downloaded by University of Warwick on 5/6/2020 11:12:47 AM.

Green Chemistry Accepted Manuscript

View Article Online
DOI: 10.1039/D0GC00544D

overall CO_2/N_2 selectivity is governed by the diffusion of gases (and the corresponding dissolved species derived from CO_2) under humid conditions.

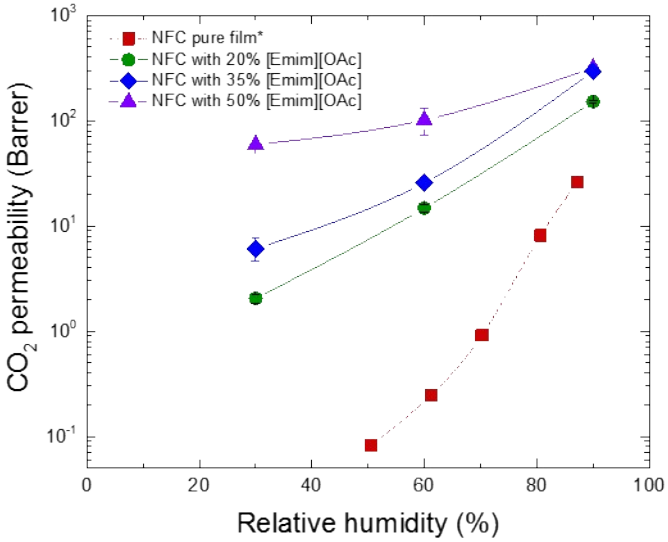

Figure 7. Humidified mixed-gas CO_2 permeability presented as a function of RH at 35°C and 1.7 bar for hybrid NFC/IL films (see legend for specimen details). (*Included for comparison are single-gas permeability results for pristine NFC membranes reported elsewhere.[5]) The solid lines serve to connect the data, and the error bars correspond to the standard error in the data.

Gate-opening mechanism for selective separation

To test our hypothesis of a size-selective separation mechanism in NFC/IL membranes that is controllable by humidity, the transport properties of noninteracting penetrant species varying in molecular size have also been tested. Single-gas permeation measurements with gases such as He and CH_4 at various RH conditions have been performed to examine the dominant role of diffusion selectivity. In these cases, **Figure 8** confirms that the selectivity of CO_2 relative to other gases depends on the kinetic diameter of the second gas and its solubility along the NFC/IL interface, which is influenced by the surrounding water activity. Given that both N_2 and He possess limited solubility in NFC/IL membranes, a large permeability difference signifies the existence of molecular transport based on size exclusion. In **Figures 8a** and **8b**, NFC-based membranes with 20 and 35 wt% [Emim][OAc], respectively, consistently possess the lowest CO_2/He ideal selectivity (between ~4 and 16) at all RH levels examined, verifying

Published on 06 May 2020. Downloaded by University of Warwick on 5/6/2020 11:12:47 AM.

Green Chemistry Accepted Manuscript

View Article Online
DOI: 10.1039/D0GC00544D

that He permeates through the membranes faster than N_2 due to its smaller kinetic diameter. In the case of CO_2/CH_4, the ideal selectivity is as high as ~100, but is generally lower than that for CO_2/N_2. Although the solubility of CH_4 in the NFC/IL membranes is expected to be higher compared to N_2 (as well as He), its size still plays a major role in contributing to a lower CO_2 selectivity relative to N_2 as a consequence of the permeation barrier afforded by the semicrystalline NFC network.

While RH affects the magnitude of these selectivities, two trends are especially noteworthy. The first is that, at low RH (30%), the CO_2/N_2 and CO_2/CH_4 ideal selectivities are comparable at both IL loading levels, suggesting that insufficient water is available for diffusion of CO_2 along contiguous pathways of IL/water in the membrane, establishing the importance of water to boost CO_2 transport along the nanofibrillar interfaces. At higher RH levels, however, the CO_2/CH_4 ideal selectivity is consistently lower than that for CO_2/N_2, and both selectivities exhibit a maximum at 60% RH. The former observation signifies that the NFC/IL membrane regulates permeation on the basis of molecular size at these conditions where the effect is pronounced to a larger extent with non-soluble N_2 than with slightly-soluble CH_4. Since the crystals comprising NFC nanofibrils constitute a natural barrier to gas permeation, it stands to reason that they are likewise responsible for sieving penetrant molecules, but to a lesser extent, in water-swollen NFC/IL membranes. The density of semicrystalline NFC nanofibrils is controlled by the IL loading level and humidity, which can be independently used to tune both gas-permeation pathways and physical obstacles within NFC/IL membranes and, in turn, the ability of these unique membranes to transport gas molecules selectively.

Published on 06 May 2020. Downloaded by University of Warwick on 5/6/2020 11:12:47 AM.

Green Chemistry Accepted Manuscript

View Article Online
DOI: 10.1039/D0GC00544D

Published on 06 May 2020. Downloaded by University of Warwick on 5/6/2020 11:12:47 AM.

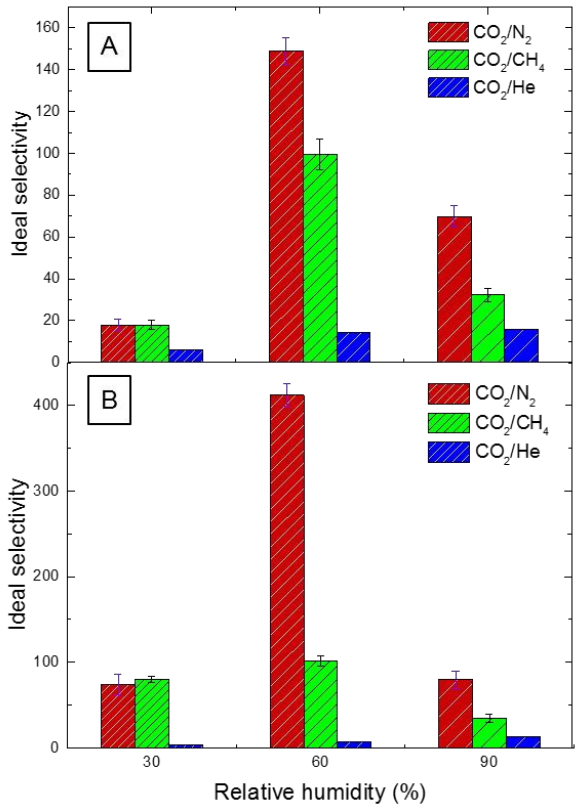

Figure 8. Ideal selectivity values of different gas pairs (see legends for specimen details) at 35°C in hybrid NFC/IL membranes at different IL loading levels (in wt%): **(A)** 20 and **(B)** 35. The error bars correspond to the standard error in the data.

Humidity-controlled permeation regimes

The mixed-gas permeation response of select NFC/IL hybrid membranes to humidity changes has been investigated in detail by using mixed-gas permeation tests, as presented in **Figure 9**. These results can effectively be divided on the basis of RH into three regimes, which are identified in **Figure 9** and schematically depicted in **Figure 10**. In the first regime ("gas-barrier"), the impenetrability of semicrystalline NFC nanofibrils dominates in **Figure 9** when the humidity level in the matrix is insufficient to swell the NFC/IL membranes and form contiguous IL/water channels. Here, penetrant transport is largely thwarted by an effective barrier membrane, and CO_2 transport depends on a combination of chemisorption of CO_2 in IL and surface diffusion of CO_2 along the viscous NFC/IL interface (which is not highly swollen

Green Chemistry Accepted Manuscript

View Article Online
DOI: 10.1039/D0GC00544D

at this RH). For this reason, CO_2 permeability depends sensitively on IL content in the matrix, increasing with an increase in the IL loading level (from ~5 Barrer at 35 wt% IL to ~60 Barrer at 50 wt% IL at 30% RH and 35ºC). Under these conditions, the CO_2/N_2 separation factor is quantitatively similar for both NFC/IL membranes due to concurrently reduced CO_2 and N_2 permeation (recalling the barrier efficacy of NFC). The second regime ("gate-opening") identified in **Figures 9** and **10** marks the condition at which sufficient membrane humidification permits swelling of NFC due to water uptake and subsequent formation of contiguous IL/water channels along the NFC nanofibrillar surfaces. In these channels, CO_2 transport is enhanced due to a combination of higher solubility and faster diffusion relative to N_2. In this scenario, the nanofibrils physically separate due to water-induced disruption of interfibrillar hydrogen-bonding. When the humidity is increased beyond 45% RH, the CO_2 permeability of the matrix starts to increase (to ~26 or ~82 Barrer for membranes with 35 or 50 wt% [Emim][OAc], respectively, with little or no change in N_2 permeability at 60% RH). This behavior is attributed to the reduced matrix viscosity and consequently enhanced diffusion of CO_2 and associated complexes, even though the partially swollen NFC still acts as a size-exclusion barrier to non-interacting and larger molecules.

In this "gate-opening" regime, CO_2 permeation is mainly governed by (*i*) faster diffusion due to the smaller kinetic diameter of CO_2 (0.33 nm) relative to N_2 (0.36 nm) and CH_4 (0.38 nm) and (*ii*) expedited transport through the IL/water layer that envelops the NFC nanofibrils and regulates molecular transport on the basis of size-exclusion. Thus, the separation factor in **Figure 9** catapults to over 370 in membranes containing 35 wt% [Emim][OAc] at 60% RH. A somewhat counterintuitive feature of the results presented in this figure is that this abrupt increase in CO_2/N_2 selectivity remains evident, but becomes less pronounced, when the IL loading level is increased to 50 wt%. Possible explanations for this unexpected result are that a higher concentration of IL further swells (and thus separates) the NFC nanofibrillar network

Published on 06 May 2020. Downloaded by University of Warwick on 5/6/2020 11:12:47 AM.

Green Chemistry Accepted Manuscript

View Article Online
DOI: 10.1039/D0GC00544D

Published on 06 May 2020. Downloaded by University of Warwick on 5/6/2020 11:12:47 AM.

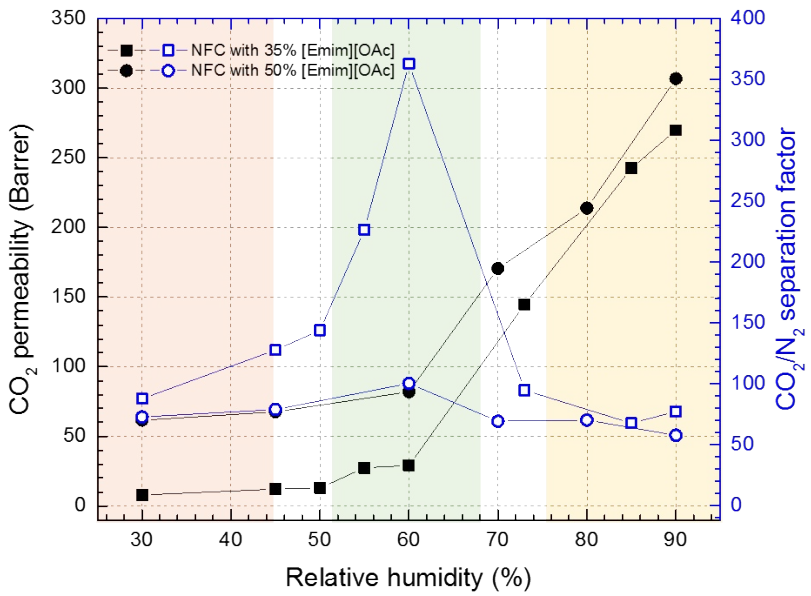

Figure 9. Humidified mixed-gas CO_2 permeability (black, left axis) and CO_2/N_2 separation factor (blue, right axis) for two hybrid NFC/IL membranes (see legend for specimen details) presented as functions of RH measured at 35°C and 1.7 bar. The shading differentiates the regimes identified in the text, and the solid lines serve to connect the data.

and, by doing so, decreases the viscosity of the matrix particularly in the IL/water region along the NFC surface, thereby yielding a more highly dilated NFC network that effectively reduces the barrier efficacy afforded by the semicrystalline nanofibrils. In similar fashion, further addition of water at higher RH levels causes the NFC/IL membranes to enter the third regime ("mechanical reinforcement") characterized by considerable swelling as they reach their maximum water uptake capacity, while the semicrystalline network of fibrils functions to reinforce the swollen matrix and hence maintain the mechanical properties of the membrane. Under these conditions, a continuous pathway of IL+water and bulk water yields high sorption and fast diffusion of CO_2, which consequently raises the CO_2 permeability to as high as 330 Barrer in membranes with 50 wt% [Emim][OAc] at 90% RH. In such highly swollen NFC/IL membranes, the resistance to N_2 diffusion is lowered significantly, leading to a less effective sieving and, consequently, to a reduced CO_2/N_2 separation factor (~58.2 at 90% RH). In these predominantly IL/water-containing membranes, the semicrystalline NFC nanofibrils serve a

Green Chemistry Accepted Manuscript

View Article Online
DOI: 10.1039/D0GC00544D

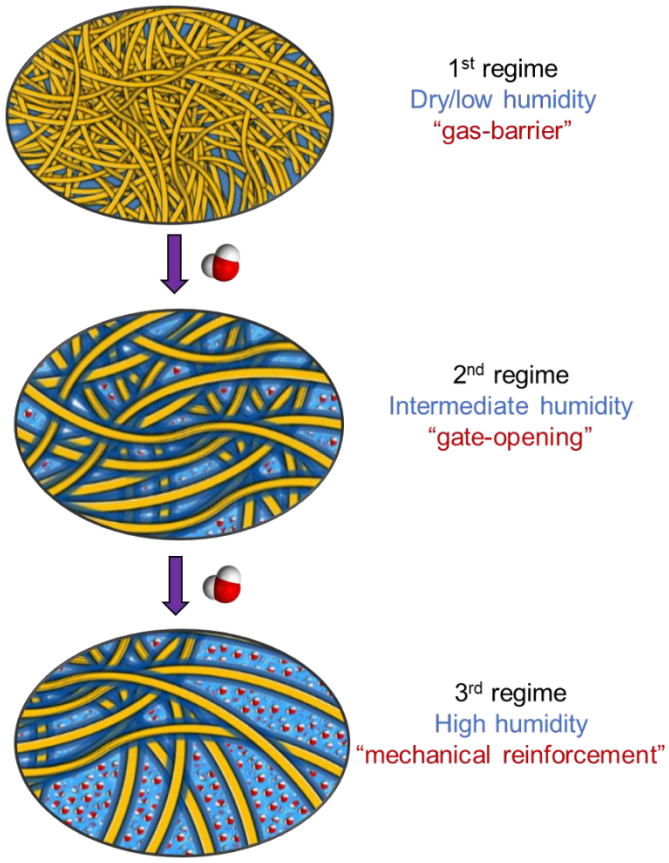

Figure 10. Illustration of nanofibrillar network dilation in hybrid NFC/IL membranes at different RH levels. Water-induced swelling in these regimes regulates CO_2 transport at constant IL loading.

different purpose by affecting bulk mechanical properties.[43]

The mechanical reinforcement of NFC in the presence of IL illustrated in **Figure 10** is established in **Figure S2** in the **Supporting Information** and is also highly beneficial in stabilizing water-swollen membranes for long-term operation, as demonstrated in **Figure S5**. Moreover, such membranes tend not to be susceptible to fluctuations in feed conditions due to their high water-retention capacity, which is consistent with results from a previous study.[4] The NFC/IL membranes fabricated and characterized in this study at different humidity levels are benchmarked in terms of their separation performance relative to the Robeson upperbound[23] in **Figure 11**. This upper bound identifies the empirical trade-off between CO_2 permeability and, in the present case, CO_2/N_2 selectivity obtained from compiled data of numerous membrane materials, thereby setting aspirational targets for new membrane performance levels to increase

Published on 06 May 2020. Downloaded by University of Warwick on 5/6/2020 11:12:47 AM.

Green Chemistry Accepted Manuscript

View Article Online
DOI: 10.1039/D0GC00544D

energy and cost efficiency of CO_2 separation systems. In general, an increase in permeability (separation throughput) is accompanied by a reduction in selectivity (separation quality) and *vice-versa*. This trade-off essentially reflects either a reduction in gas selectivity as all penetrant molecules migrate under comparable conditions of obstruction through a dense membrane or an increase in gas selectivity as molecular transport (usually associated with diffusion) becomes generally more difficult and species-differentiated. As anticipated from the described mechanisms governing gas transport different regimes in **Figures 9** and **10**, all the NFC/IL membranes exhibiting water-induced gate-opening for CO_2 at intermediate RH levels transcend the upper bound. As far as we are aware, this is the first example of a water-swollen nanofibrillated membrane to exhibit such remarkable CO_2-separation performance. Even without the apparently unique mechanism associated with molecular gate-opening, highly humidified NFC/IL membranes are capable of efficiently separating CO_2 from N_2, as evidenced

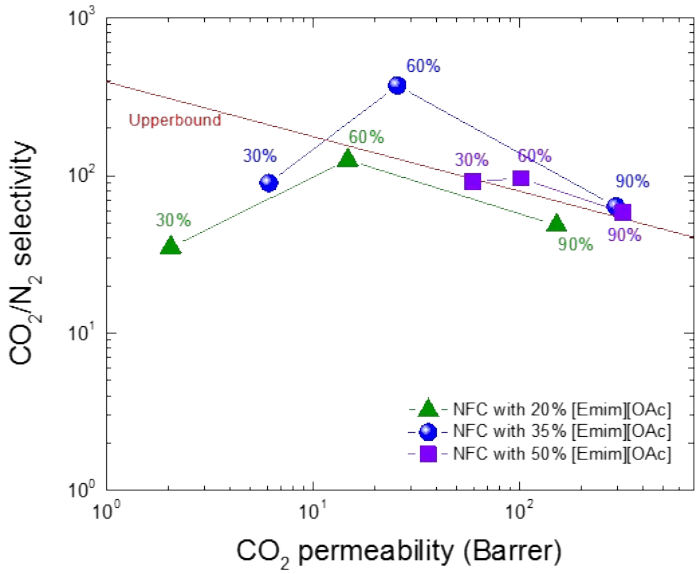

Figure 11. Gas-separation performance of humidified NFC/IL membranes (see legend for specimen details) at various RH conditions at 35°C relative to the Robeson upper bound (red line).[23] The solid lines serve to connect the data, and the RH level is assigned to each datum point.

by their close proximity to the upper bound, thereby confirming that these eco-friendly membranes with high CO_2 permeability and competitive CO_2/N_2 selectivity capabilities are

Published on 06 May 2020. Downloaded by University of Warwick on 5/6/2020 11:12:47 AM.

Green Chemistry Accepted Manuscript

View Article Online
DOI: 10.1039/D0GC00544D

aptly suitable for gas-separation applications related to carbon capture and ultimately mitigating climate change.

Conclusions

The current work concurrently exploits the gas-barrier property of NFC nanofibrils in the presence of an incorporated IL to generate a new generation of hybrid membranes that are humidity-tunable and highly permeable/selective for the purpose of CO_2 separation. In fact, the biological origin and hydrophilicity of nanocellulose in conjunction with the use of an IL as a eco-friendly additive in these hybrid membranes yields "green" membranes with tremendously promising separation properties. This class of membranes not only exhibits CO_2 permeability and CO_2/N_2 selectivity levels that reside near or exceed the Robeson upper bound but also reveals the existence of multiple transport mechanisms that are governed by water-induced nanoscale changes in NFC packing, which effectively dictates gas transport on the basis of molecular size. In particular, we identify three different humidity-driven regimes wherein (*i*) molecular transport is generally restricted and CO_2 diffusion depends strongly on IL loading, (*ii*) CO_2 transport is greatly enhanced by the presence of contiguous IL+water channels that open the gate for CO_2 while still restricting the diffusion of larger molecules, and (*iii*) non-differentiated molecular transport occurs quickly (high permeabilities) at reduced selectivity. In this regard, both IL loading and humidity serve as independent external controls that can be used to regulate gas-transport properties of NFC. This study demonstrates the largely unexplored potential of 1D semicrystalline nanofibrils as adjustable, semi-permeable size-sieving membranes capable of affording precise control over network characteristics and, hence, size exclusivity in bio-based gas-separation membranes. Under optimal IL loadings and/or humidity levels, these green membranes showcase CO_2/N_2 selectivities as high as ~370 and CO_2 permeabilities as high as ~330 Barrer, clearly demonstrating their potential for application in CO_2 separation.

Published on 06 May 2020. Downloaded by University of Warwick on 5/6/2020 11:12:47 AM.

Green Chemistry Accepted Manuscript

View Article Online
DOI: 10.1039/D0GC00544D

Published on 06 May 2020. Downloaded by University of Warwick on 5/6/2020 11:12:47 AM.

Green Chemistry Accepted Manuscript

Conflicts of Interest

The authors declare no conflicts of interest.

Acknowledgments

This work is part of the NANOMEMC2 project, and the authors acknowledge the financial support from the EU Horizon 2020 Research and Innovation program under Grant Agreement n° 727734. The Research Council of Norway is acknowledged for support of the Norwegian Micro- and Nano-Fabrication Facility, NorFab, under project number 245963/F50. Authors at NC State University are grateful to the Eastman Center of Excellence for financial support. Dr. K. Missoum and Dr. M. Alves from INOFIB S.A.S. are acknowledged for providing the nanocellulose. We thank Dr. S. Evjen and Professor A. Fiksdahl for assistance with screening ILs, Dr. M. Manikandan for the EDS measurements, and Professor H. B. Park and Ms. J. S. Ah for the XPS characterization.

References

1 A. Dufresne, *Mater. Today*, 2013, **16**, 220–227.

2 N. Lavoine, I. Desloges, A. Dufresne and J. Bras, *Carbohydr. Polym.*, 2012, **90**, 735–764.

3 B. Thomas, M. C. Raj, B. K. Athira, H. M. Rubiyah, J. Joy, A. Moores, G. L. Drisko and C. Sanchez, *Chem. Rev.*, 2018, **118**, 11575–11625.

4 S. Janakiram, X. Yu, L. Ansaloni, Z. Dai and L. Deng, *ACS Appl. Mater. Interfaces*, 2019, **11**, 33302–33313.

5 L. Ansaloni, J. Salas-Gay, S. Ligi and M. G. Baschetti, *J. Membr. Sci.*, 2017, **522**, 216–225.

6 D. Venturi, L. Ansaloni and M. G. Baschetti, *Chem. Eng. Trans.*, 2016, **47**, 349–354.

7 D. Venturi, D. Grupkovic, L. Sisti and M. G. Baschetti, *J. Membr. Sci.*, 2018, **548**, 263–274.

View Article Online
DOI: 10.1039/D0GC00544D

8 Z. Dai, J. Deng, Q. Yu, R. M. L. Helberg, S. Janakiram, L. Ansaloni and L. Deng, *ACS Appl. Mater. Interfaces*, 2019, **11**, 10874–10882.

9 J. Torstensen, R. M. L. Helberg, L. Deng, Ø. W. Gregersen and K. Syverud, *Int. J. Greenh. Gas Control*, 2019, **81**, 93–102.

10 C. Aulin, S. Ahok, P. Josefsson, T. Nishino, Y. Hirose, M. Österberg and L. Wågberg, *Langmuir*, 2009, **25**, 7675–7685.

11 Y. Habibi, *Chem. Soc. Rev.*, 2014, **43**, 1519–1542.

12 M. Isik, H. Sardon and D. Mecerreyes, *Int. J. Mol. Sci.*, 2014, **15**, 11922–11940.

13 H. Wang, G. Gurau and R. D. Rogers, *Chem. Soc. Rev.*, 2012, **41**, 1519.

14 S. Velioglu, X. Yao, J. Devémy, M. G. Ahunbay, S. B. Tantekin-Ersolmaz, A. Dequidt, M. F. Costa Gomes and A. A. H. Pádua, *J. Phys. Chem. B*, 2014, **118**, 14860–14869.

15 B. Lam, M. Wei, L. Zhu, S. Luo, R. Guo, A. Morisato, P. Alexandridis and H. Lin, *Polymer*, 2016, **89**, 1–11.

16 Z. Dai, R. D. Noble, D. L. Gin, X. Zhang and L. Deng, *J. Membr. Sci.*, 2016, **497**, 1–20.

17 Z. Dai, L. Ansaloni, J. J. Ryan, R. J. Spontak and L. Deng, *Green Chem.*, 2018, **20**, 1391–1404.

18 M. Minelli, M. G. Baschetti, F. Doghieri, M. Ankerfors, T. Lindström, I. Siró and D. Plackett, *J. Membr. Sci.*, 2010, **358**, 67–75.

19 Y. Zhang, J. Sunarso, S. Liu and R. Wang, *Int. J. Greenh. Gas Control*, 2013, **12**, 84–107.

20 Y. Peng, Y. Li, Y. Ban, H. Jin, W. Jiao, X. Liu and W. Yang, *Science*, 2014, **346**, 1356–1359.

21 M. Ahmadi, S. Janakiram, Z. Dai, L. Ansaloni and L. Deng, *Membranes.*, 2018, **8**, 50.

22 S. Janakiram, M. Ahmadi, Z. Dai, L. Ansaloni and L. Deng, *Membranes*, 2018, **8**, 24.

23 L. M. Robeson, *J. Membr. Sci.*, 2008, **320**, 390–400.

Published on 06 May 2020. Downloaded by University of Warwick on 5/6/2020 11:12:47 AM.

Green Chemistry Accepted Manuscript

View Article Online
DOI: 10.1039/D0GC00544D

24 L. Ansaloni, R. Rennemo, H. K. Knuutila and L. Deng, *J. Membr. Sci.*, 2017, **537**, 272–282.

25 M. Minelli, G. Cocchi, L. Ansaloni, M. G. Baschetti, M. G. De Angelis and F. Doghieri, *Ind. Eng. Chem. Res.*, 2013, **52**, 8936–8945.

26 M. Chiara Ferrari, M. Galizia, M. G. De Angelis and G. Cesare Sarti, *Membr. Gas Sep.*, 2010.

27 J. Crank, *The Mathematics of Diffusion. 2nd Ed.*, Clarendon Press, Oxford, 1979.

28 J. Catalano, T. Myezwa, M. G. De Angelis, M. G. Baschetti and G. C. Sarti, *Int. J. Hydrogen Energy*, 2012, **37**, 6308–6316.

29 Y. Chen, X. Sun, C. Yan, Y. Cao and T. Mu, *J. Phys. Chem. B*, 2014, **118**, 11523–11536.

30 X. Tan, X. Li, L. Chen and F. Xie, *Phys. Chem. Chem. Phys.*, 2016, **18**, 27584–27593.

31 M. Salajkova, L. Valentini, Q. Zhou and L. A. Berglund, *Compos. Sci. Technol.*, 2013, **87**, 103–110.

32 A. J. Svagan, M. A. S. Azizi Samir and L. A. Berglund, *Biomacromol.*, 2007, **8**, 2556–2563.

33 M. Henriksson, L. A. Berglund, P. Isaksson, T. Lindström and T. Nishino, *Biomacromol.*, 2008, **9**, 1579–1585.

34 R. Sharma, V. K. Varshney, G. S. Chauhan, S. Naithani and P. L. Soni, *J. Appl. Polym. Sci.*, 2009, 113, 2450–2455.

35 M. T. Clough, K. Geyer, P. A. Hunt, J. Mertes and T. Welton, *Phys. Chem. Chem. Phys.*, 2013, **15**, 20480–20495.

36 J. Torstensen, M. Liu, S. A. Jin, L. Deng, A. I. Hawari, K. Syverud, R. J. Spontak and Y. W. Gregersen, *Biomacromol.*, 2018, **19**, 1016–1025.

37 M. Moreno, F. Castiglione, A. Mele, C. Pasqui and G. Raos, *J. Phys. Chem. B*, 2008, **112**, 7826–7836.

38 L. Deng, T. J. Kim and M. B. Hägg, *J. Membr. Sci.*, 2009, **340**, 154–163.

39 D. Chinn, D. Q. Vu, M. S. Driver and L. C. Boudreau, *U.S. Patent* 7,527,775, May 5,

Published on 06 May 2020. Downloaded by University of Warwick on 5/6/2020 11:12:47 AM.

Green Chemistry Accepted Manuscript

View Article Online
DOI: 10.1039/D0GC00544D

2009.

40 G. Gurau, H. Rodríguez, S. P. Kelley, P. Janiczek, R. S. Kalb and R. D. Rogers, *Angew. Chem. Int. Ed.*, 2011, **50**, 12024–12026.

41 L. Gómez-Coma, A. Garea and Á. Irabien, *ACS Sustain. Chem. Eng.*, 2017, **5**, 734–743.

42 S. Fendt, S. Padmanabhan, H. W. Blanch and J. M. Prausnitz, *J. Chem. Eng. Data*, 2011, **56**, 31–34.

43 E. Jiang, N. Amiralian, M. Maghe, B. Laycock, E. McFarland, B. Fox, D. J. Martin and P. K. Annamalai, *ACS Sustain. Chem. Eng.*, 2017, **5**, 3296–3304.

44 H. Bux, C. Chmelik, J. M. Van Baten, R. Krishna and J. Caro, *Adv. Mater.*, 2010, **22**, 4741–4743.

45 I. Kikic, M. Lora, A. Cortesi and P. Sist, *Fluid Phase Equilib.*, 1999, **158**, 913–921.

46 A. Yokozeki, M. B. Shiflett, C. P. Junk, L. M. Grieco and T. Foo, *J. Phys. Chem. B*, 2008, **112**, 16654–16663.

47 L. Segal, J. J. Creely, A. E. Martin Jr. and C. M. Conrad, *Text. Res. J.*, 1959, 786–794.

Published on 06 May 2020. Downloaded by University of Warwick on 5/6/2020 11:12:47 AM.

Green Chemistry Accepted Manuscript